Lab on a Chip



Cite this: Lab Chip, 2011, 11, 1664

www.rsc.org/loc PAPER

Highly sensitive fluorescence detection system for microfluidic lab-on-a-chip

Gihan Ryu, Jingsong Huang, Oliver Hofmann, Claire A. Walshe, Jasmine Y. Y. Sze, Gareth D. McClean, Alan Mosley, Simon J. Rattle, John C. deMello, Andrew J. deMello and Donal D. C. Bradley

Received 11th November 2010, Accepted 28th February 2011 DOI: 10.1039/c0lc00586j

We demonstrate a compact, low cost and practical fluorescence detection system for lab-on-a-chip applications. The system comprises a commercially available InGaN light emitting diode (501 nm) as light source, an organic or silicon photodiode detector, absorptive dye coated colour filters and linear and reflective polarisers. An injection moulded polystyrene microfluidic chip is used as the platform for fluorescence immunoassays for cardiac markers myoglobin and CK-MB. The optical limit of detection (LOD) is measured using a TransFluoSphere® suspension at 5.6×10^4 beads μ l⁻¹ which can be equated to \sim 3 nM fluorescein equivalent concentration. The LOD for the human plasma immunoassays is measured as 1.5 ng ml⁻¹ for both myoglobin and CK-MB.

1. Introduction

Modern life styles encourage people to be more health conscious, an objective that would be helped by the availability of simple, low-cost tests for monitoring existing conditions, screening for other disease states 1-3 and increasing the involvement of patients in their own care.4 Development of commercial tests are, however, dependent on technological progress to ensure that point of care testing (POCT) provides results of a quality and reliability comparable with those from the laboratory. Improvements in microfluidic chip technology have contributed to the development of in vitro diagnostic tests that are suitable for self-testing and make miniaturisation of the test system possible. Various detection methods in combination with microfluidic chip technology have been reported, for example fluorescence, 5-11 absorbance, 12,13 chemiluminescence, 14-18 refractive index change (interferometric 19-23 and surface plasmon resonance 24-26) and Raman spectroscopy.27

Fluorescence is one of the most commonly used and well developed analytical methods applied within biotechnology but the detection technology is optimised for use in the laboratory environment. Most fluorescence measurement systems use bulky, complex and expensive optical components such as microscopes, lasers, interference band pass filters, monochromators, CCD cameras and/or photomultiplier tubes. They are, consequently, incompatible with the requirements of POCT devices, in particular with regard to being compact, preferably hand-held sized,

and low-cost analysis tools. We^{10,11,14–16,29} and several other groups have reported ways of miniaturising the package size and of reducing costs. For example Novak *et al.* reported a low cost and compact design for fluorescence detection by using an LED light source and photodiode (PD) detector,²⁸ and Pais *et al.* presented a disposable lab-on-a-chip (LOC) using an organic light emitting diode (OLED) and organic photodiode (OPD) system with crossed polarisers.⁷ Other approaches were also tried by integrating functions such as the microfluidic chip and colour filters,²⁹ microfluidic chip and waveguide⁵ and monolithic integration of LED and PD.⁹ These new technologies are very much works in progress and it will be some time before they mature.

In this paper, we demonstrate a compact, practical and low cost fluorescence detection system that can be applied to POCT and present its application to two prototype tests commonly used in the early diagnosis of myocardial infarction: myoglobin and CK-MB.

2. Detection system

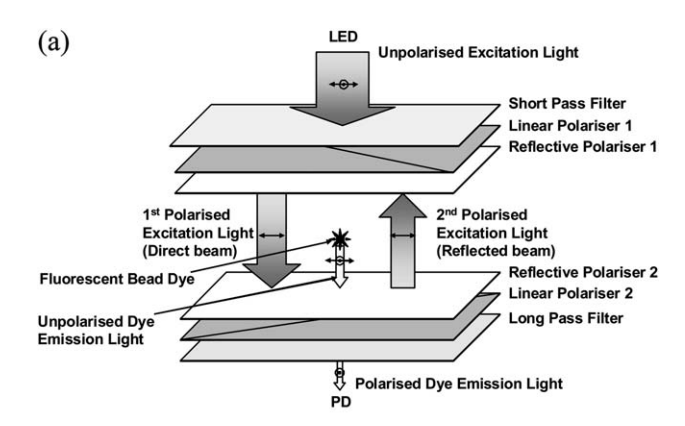
2.1. System design and characterisation

A schematic diagram of the fluorescence detection system is depicted in Fig. 1. The optical configuration for the fluorescence detection system depends on the fluorescent label used for the immunoassays and here we have designed the system for a bluegreen light absorbing and red light emitting fluorescence bead (see Experimental section for details). A green LED (Osram Opto Semiconductors, LV E63C-BBDA-35) is used as the excitation light source; this emits at a peak wavelength $\lambda = 501$ nm (full width half maximum (FWHM) $\Delta\lambda = 30$ nm) with $\pm 20^\circ$ divergence angle determined by the in-built package lens. Selection of the LED was based on compatibility with the optical properties of the fluorophore used for the immunoassays and to minimise fluorescence interference from the test sample (human serum). The luminous intensity reaches 1940 mcd at 3.8 V and 30 mA,

^aMolecular Vision Ltd. BioIncubator Unit, Bessemer Building, Imperial College London, London, SW7 2BP, UK. E-mail: simon.rattle@molecularvision.co.uk

^bDepartment of Chemistry and Centre for Plastic Electronics, Imperial College London. London. SW7 2AZ. UK

^cDepartment of Physics and Centre for Plastic Electronics, Blackett Laboratory, Imperial College London, London, SW7 2AZ, UK. E-mail: d.bradley@imperial.ac.uk



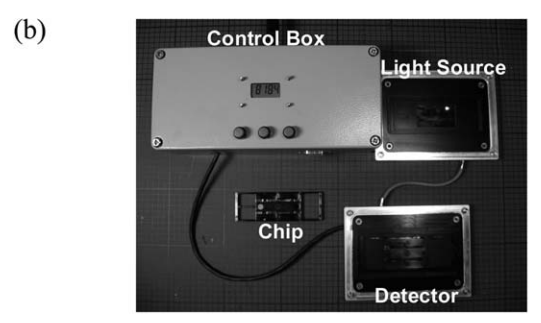


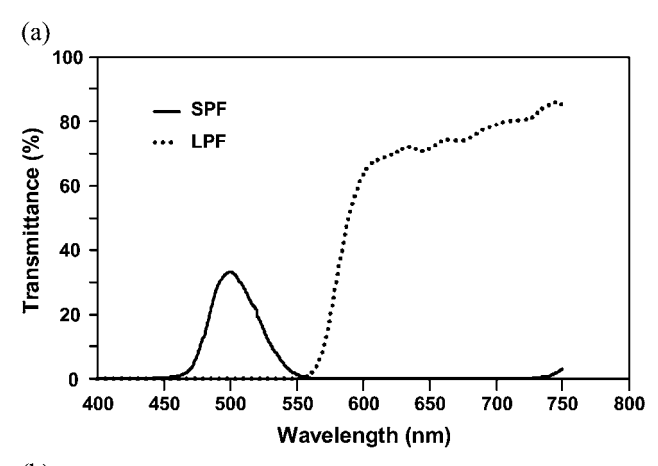
Fig. 1 (a) Schematic diagram of the fluorescence detection system used in our microfluidic structures. Light propagation is depicted in the diagram by the vertical single-headed arrows (pointing in the direction of travel), where the size of the arrow represents the relative light intensity (not to scale). The polarization of the propagating light is indicated by the horizontal double-headed arrows (polarization in the plane of the paper) and by the centred circles (polarization out of the plane of the paper). LED stands for light emitting diode and PD for photodiode. (b) A photograph of the device structure we have used. The light source and detector are mounted on two flanges that join together face-to-face to form a light tight enclosure during measurement. These flanges are recessed to accurately locate the chip in the light path between the source and detector.

equivalent to a luminance of 180 kcd m⁻². The LED has an unwanted weak emission component tailing into the red (see Fig. 3) that has the potential to interfere with the immunoassay fluorescence signal. The optical system described here therefore contains three filtering components sandwiching the sample volume and designed to limit the influence of this light: a matched pair of short and long pass absorptive filters, a pair of crossed linear polarisers and a pair of crossed reflective polarisers.

The short pass filter (SPF, Lee Filters) and long pass filter (LPF, Lee Filters) are approximately 70 μm thick absorption dye coated plastic films; their transmittance spectra are shown in Fig. 2(a). Lee Filters' SPF and LPF are low cost (<10 pence per cm²) materials but in each case the cut-off is not as sharp as seen with interference filters. The SPF has a Gaussian-like-shape transparency window with peak transmission 30% at 500 nm and FWHM 40 nm. It is a relatively effective light blocker (transmission $\leq 0.1\%$) for wavelengths in the 600–700 nm region with increasing light leakage apparent beyond 725 nm. The LPF is blocking at short wavelengths and then becomes transparent for $\lambda > 570$ nm. The SPF reduces the excitation light intensity overall by approximately 70% but in the light emitting region of the

fluorescence bead (570–660 nm) the suppression is more dramatic (Fig. 2(b)). Because the fluorescence emission intensity of the target sample is normally very weak compared to the excitation light intensity, suppression of the tail part of the excitation light is an important factor to increase the signal to noise ratio and to improve the limit of detection (LOD). The LPF further helps to discriminate the signal from any excitation light background.

Two orthogonally aligned ('crossed') linear polarizers (Nitto-Denko, NPF-SEG1425DU) were used to further reduce the excitation light background that reaches the detector. The polarizer film is about 200 µm in thickness and has a polarization discrimination ratio of 1/1900 across most of the visible spectrum but the ratio decreases significantly for $\lambda > 650$ nm. With each linear polarizer having transmittance $\sim 40\%$ there are disadvantages in the loss of excitation light delivered to and fluorescence signal collected from the sample. There is a major advantage, however, in the enhanced suppression of excitation leakage light (Fig. 3). The combination of SPF and LPF (dotted line) alone reduces the background excitation light by a factor of 105 at 530 nm and 600 nm with the imperfect cutoff of the colour filters responsible for much of the residual leakage. Use of the crossed polariser system together with the colour filters (solid line) allows suppression of leakage light by a total factor of 108 at 530 nm and 106 at 600 nm.



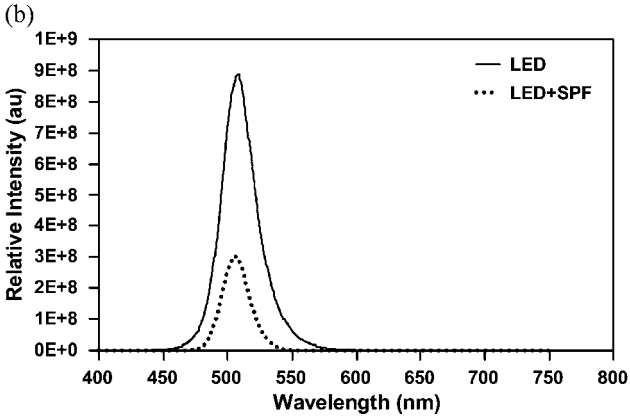


Fig. 2 (a) Transmittance spectra of the short pass filter (SPF, solid line) and long pass filter (LPF, dotted line). These filters are absorbance type dye deposited plastic films. (b) The emission spectra of the green light emitting diode excitation light source, without (solid line) and with (dotted line) the short pass filter inserted in the optical path to the detector.

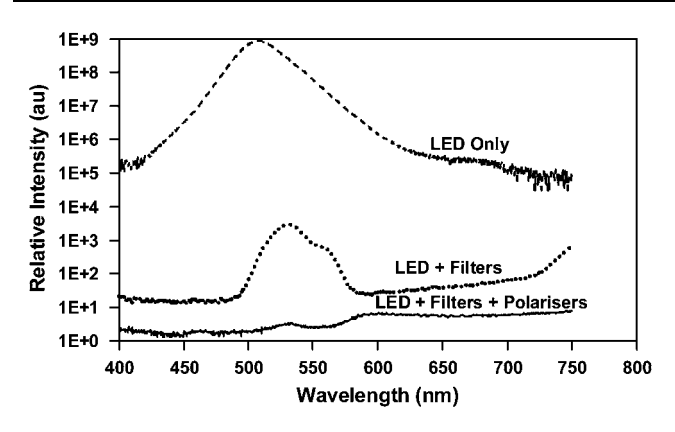


Fig. 3 Suppression of LED background leakage. LED emission (dashed line) peaks at 501 nm but there is a significant tail extending beyond 600 nm. Use of the SPF and LPF filter combination (dotted line) allows a 10⁵-fold suppression of background light intensity at 530 nm and at 600 nm. Addition of the crossed polarizer combination (solid line) allows, in total, 10⁸-fold suppression at 530 and 10⁶ at 600 nm.

The reflective polariser film (3M, dual brightness enhancement film (DBEF)) is commonly used in liquid crystal displays (LCDs) to increase the brightness by recycling light that would otherwise be absorbed in the rear polariser. DBEF comprises a multilayer distributed Bragg reflector containing a birefringent material that ensures a high reflectivity for one linear polarization of incident light. The other polarization is efficiently transmitted. In Fig. 1 linear polariser 1 and reflective polariser 1 are aligned in parallel so that the excitation light that passes through linear polariser 1 will also be transmitted by reflective polariser 1. However, reflective polariser 2 is aligned orthogonal to reflective polariser 1 so the light transmitted by reflective polariser 1 is reflected back into the sample volume from the surface of reflective polariser 2. This reflected light can excite the fluorescent bead sample on its second pass, offsetting in part the initial attenuation of the excitation light within the absorptive linear polariser 1. Reflective polariser 1 can further enhance the collection of fluorescence from within the sample volume since any signal reflected from this polariser will have the right polarisation to pass through reflective polariser 2 and linear polariser 2 on its way to the detector.³⁰ In principle it would be possible to omit the absorptive linear polarisers from our detection scheme altogether but only were it possible to increase the polarisation discrimination ratio for the reflective polarisers—something that is not expected to be trivial. It is for that reason that we utilise both the absorptive and reflective polarisers. Another enhancement would be to use a polarised emission LED, something that can be achieved with uniaxially aligned conjugated polymers emitting in the blue and green/yellow. 31,32

Whilst the use of polarised light has attractions for controlling excitation light leakage one concern is in relation to the accuracy of alignment required of the polarisers. Fig. 4 shows the calculated and measured amount of leakage light, normalised to its minimum level, as a function of the misalignment angle for the polariser (combined linear and reflective polarisers). A small degree of misalignment results in a significant increase—for example a 2° misalignment gives a three-fold increase—in light leakage. Clearly, there is then a need for accurate alignment of the polarisers during system integration.

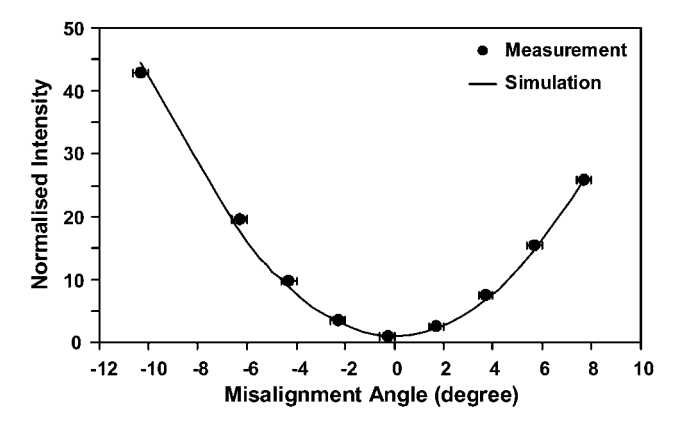
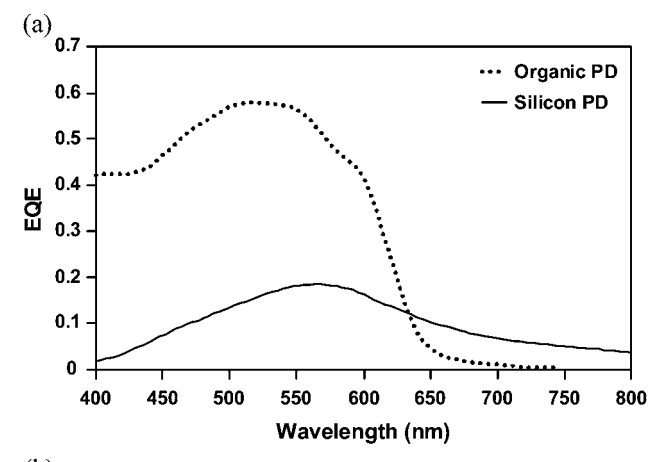


Fig. 4 Excitation light intensity leaking through to the photodiode as a consequence of misalignment between the polarisers (linear and reflective combined polarisers). The data points represent measured values with the solid line the calculated dependence.

The fluorescence detection system we use has no element, for example an interference filter or diffraction grating, to spectrally select the light incident on the photodiode. All photons that are absorbed by the photodiode will contribute to the measured electric current. Hence, the residual leakage light (solid curve in Fig. 3) sets a detection floor below which a true signal cannot be discriminated from the background. However, as we show below, the levels of background rejection that we reach are sufficient to undertake sensitive immunoassays.

To address the needs of POCT, we compared the use of an organic PD with that of a low cost commercially available large area silicon PD that was selected to have a similar spectral response to that of the organic PD. Fig. 5(a) shows the external quantum efficiency (EQE) spectra of both organic (bulk heteropoly(3-hexylthiophene) (P3HT):[6,6]-phenyl-C₆₁junction butyric acid-methylester (PCBM) blend based)^{16,33} and silicon (Osram Opto Semiconductors, SFH2430) photodiodes. The EQE of the organic PD exceeds 40% across the wavelength range λ 400–600 nm, with peak EQE \approx 58% at $\lambda \approx$ 520 nm. This is substantially higher than for the SFH2430 silicon PD that has a poor short wavelength response and a peak EOE $\approx 19\%$ at $\lambda \approx$ 560 nm. For $\lambda > 600$ nm the organic PD EQE rapidly decreases, crossing that of the SFH2430 silicon PD at ~640 nm and petering out beyond ~650 nm. This is a direct consequence of the absorption spectrum of the P3HT:PCBM blend.34 The SFH2430 silicon PD retains a moderate EQE (~4%) to 800 nm and beyond—its specified sensitivity range is 400 to 900 nm. Taking into account the measured residual leakage light spectrum (Fig. 3), in order to maximise the signal to noise ratio an ideal photodiode would have a band pass EQE spectrum matched to the TransFluoSphere® emission band (570–700 nm). The organic PD has a reasonably good match to this in respect of its infrared (IR) blind behaviour, albeit that this onsets at a shorter wavelength (650 nm) than desired (700 nm). It also has a relatively high EQE across a major portion of the TransFluoSphere® emission band but it retains high sensitivity for shorter wavelengths. Conversely, the silicon PD's response does not fall off fast enough beyond 700 nm and whilst it does drop for wavelengths shorter than 570 nm it again does so rather slowly. An IR blocking filter can be used to improve the situation for the silicon PD.



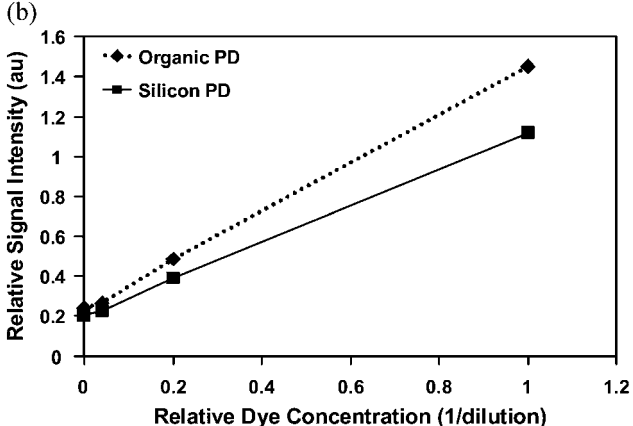


Fig. 5 (a) External quantum efficiency (EQE) spectra and (b) measured signal intensity as a function of TransFluoSphere® bead suspension concentration using the organic (dotted line, filled diamonds) and silicon with IR blocking filter (solid line, filled squares) photodiodes.

Fig. 5(b) shows the signal intensities for TransFluoSphere® suspensions of different concentrations measured using organic (dotted line) and SFH2430 silicon (solid line) PDs, the latter with the benefit of an added IR blocking filter (absorption type dye doped plastic film from Kentek). As expected (given the EQE spectra in Fig. 5(a)) the organic PD yields a larger current than the silicon PD. As yet, however, the organic PDs have not been optimized for practical small size packaging. Consequently most of the experimental data reported below were collected using the silicon PD plus infrared blocking filter. Longer term, the ability to directly integrate organic PDs with microfluidic chip structures and to utilize high-throughput low temperature manufacturing processes for PD fabrication, combined with a generally superior photoresponse, is expected to favour the adoption of organic PDs.

2.2. Microfluidic chip and assay

The microfluidic chips are made of injection moulded black polystyrene. The chip design has separate channels for each of the two analytes with each channel comprising two detection chambers. The first chamber provides a background reference while the second is used for specific sample test measurement (Fig. 6). To avoid optical interference, the detection chamber

areas in the injection moulded chips are hollow and only become enclosed after sealing of the structured and non-structured side with optically clear films. The dimensions of the microfluidic channels are 130 μ m (width) \times 200 μ m (depth) in the delay loop and 2 mm (width) \times 200 μ m (depth) in the other channel sections. The detection chamber is 2 mm (width) \times 3 mm (length) × 500 μm (depth). For the immunoassays, 1 μl volumes of fluorescent beads conjugated with antibody to the analyte are deposited in the fluid channel downstream from the reference detection zone and dried. Plasma sample or standard is loaded into the inlet and flows under passive capillary flow along the microfluidic channel, reconstituting the dried fluorescent labelled antibody. The design of the fluid channel allows time for reaction of the antigen in the sample with the labelled antibody before the fluid reaches the second detection zone where the labelled antigen is captured by a second antibody immobilised on the channel surface. Excess sample is drawn through the detection zone by a wick, thereby rinsing the detection zone of uncomplexed fluorescent beads. The resultant light measured at the detection zone is derived from fluorescent beads bound to the surface through the antibody immunocomplex and is proportional to the concentration of antigen present in the sample. Ideally this would be the sole source of light reaching the detector. In practice there is a contribution from uncomplexed fluorescent beads that are not flushed from the detection zone (non-specific binding), arising from limitations in fluid flow, and a small amount of excitation leakage light that is not blocked by the light filters.

3. Experimental

Optical limit of detection (LOD) measurements were made using the configuration shown in Fig. 1(a) with (i) a silicon PD and IR blocking filter and, for comparison, (ii) a spectroscopic detection system. The spectroscopic system is composed of an Andor SR-163 spectrograph coupled to an Andor DV420A-BV charge coupled device (CCD) camera, with optical fibre fluorescence collection and delivery to the spectrograph. Measurements were made on a dilution series of fluorescent beads (Molecular Probes Inc.,

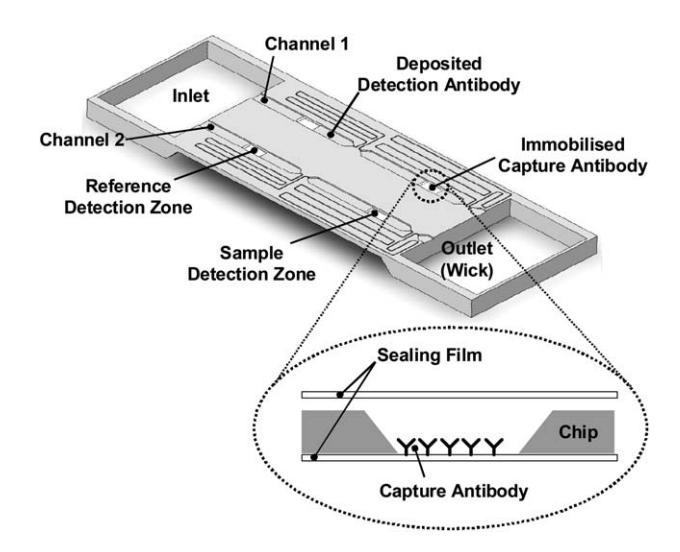


Fig. 6 Microfluidic chip design for fluorescence detection. The two test channels each have one reference and one sample detection chamber.

TransFluoSphere®, peak wavelengths of absorption and emission are 488 nm and 605 nm) in deionised (DI) water. The concentration of fluorescent beads (nominal size 100 nm) in the as supplied suspension was 10¹³ beads ml⁻¹. The dilution series was studied for suspensions within both 1 mm thickness cuvettes (for spectrum analysis) and microfluidic chips (for direct measurement).

The analytical detection limits of the immunoassays were determined separately through an assessment of the imprecision of measurement of zero analyte concentration. For these microfluidic measurements the injection moulded chips were sealed with an optically clear pressure sensitive adhesive film after deposition of the labelled and capture antibodies. Tests were run by simply applying a test sample or standard to the inlet chamber then waiting for a defined period of time to allow completion of the immunoreactions and flushing of unbound fluorescent beads from the detection zone. Calibration curves for each of myoglobin and CK-MB were constructed by measuring the system response for standard concentrations of each analyte prepared by dilution of stock antigens in myoglobin free human serum (Hytest Ltd). Estimates of the detection limit for each assay were obtained from the concentration corresponding to the mean plus three standard deviations of signal of the zero standard.

4. Results and discussion

4.1. Limit of detection (LOD)

The emission spectrum and intensity of the excitation light source are critical in determining the fluorescent bead emission intensity but sourcing a LED with optimum characteristics is difficult. Since many biological samples fluoresce when exposed to blue light, selection of a green rather than a blue LED helps to reduce problems associated with auto fluorescence raising the background light level. The chosen green LED (Osram Opto Semiconductors, LV E63C-BBDA-35) is very bright, reaching 180 kcd m⁻² luminance at 3.8 V (30 mA), but its peak emission wavelength is 501 nm (slightly longer wavelength than the peak absorption of TransFluoSphere®). In addition, the long wavelength component ($\lambda > 600$ nm) in the LED emission (see Fig. 3) extends into the emission window of the bead fluorescence so it is important to filter out this component. An LED with a more abrupt cut-off on the long wavelength side of its emission peak would be preferable.

Fig. 7 shows a set of TransFluoSphere® bead emission spectra for different suspension concentrations. Deionised water was used as a reference to measure the leakage light background level. The as supplied bead suspension (10^{10} beads μl^{-1}) was diluted in deionised water and the emission spectra were measured at four concentrations, namely 10³, 10⁴, 10⁵ and 10⁶ beads µl⁻¹. Very little light is detected between 400 nm and 550 nm when deionised water alone is used and this level does not change markedly for increasing bead concentration, consistent with this part of the spectrum being purely leakage light from the LED. The highest concentration sample has a marginally higher leakage level, possibly attributable to a small amount of polarisation scrambling by scattering. The notable fringe-like fluctuation in the leakage light level across the 400 to 550 nm wavelength range is tentatively attributed to interference effects associated with the multilayer optical structure.

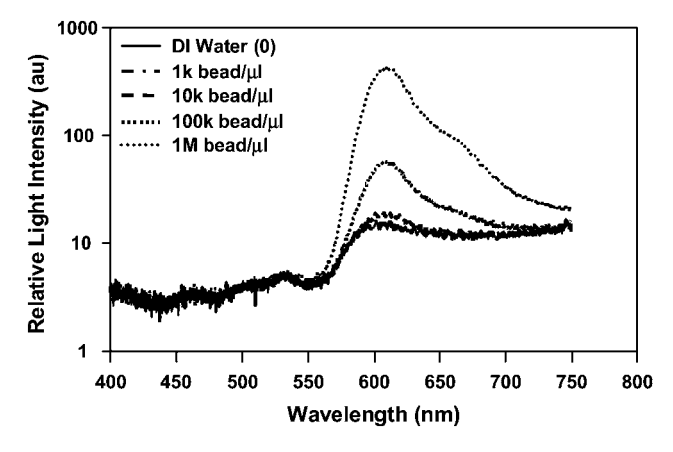


Fig. 7 Emission spectra of TransFluoSphere® suspensions of varying bead concentration excited with an Osram LV E63C-BBDA-35 LED. The emission was collected with an optical fibre, dispersed in an Andor SR-163 spectrograph and detected with an Andor DV420A-BV CCD camera. The spectrum for 10³ bead μl⁻¹ is indistinguishable from that for deionised water (no beads), which represents the leakage-excitation-light-determined baseline of the fluorescence detection system.

Beyond 550 nm the signal evolves with increasing bead concentration and the characteristic bead emission spectrum becomes evident. The leakage light level is higher in this part of the spectrum than at shorter wavelengths—undesirable in respect of the limit of detection. The spectrum measured for the lowest concentration sample (10^3 beads μ l⁻¹) is more or less indistinguishable from the deionised water reference. The next concentration sample (10^4 beads μ l⁻¹) shows a small but nevertheless discernible increase in signal. The two highest concentration samples (10^5 and 10^6 beads μ l⁻¹) show very clear emission peaks. Based on such a spectral analysis the limit of detection would be estimated to be $\leq 10^4$ beads μ l⁻¹.

However, as described above, the photodiode will absorb background leakage light as well as the TransFluoSphere® emission signal and consequently the detection limit using a photodiode without a spectral selection element will be higher than that derived from the spectrum analysis. In addition, our fluorescence detection system uses a simple PD amplifier circuit without specific treatment of the noise. Fig. 8 shows the response, as a function of TransFluoSphere® bead concentration, measured with our detection system, utilizing here the silicon PD with IR blocking filter as photodetector. The detection chamber volume was 3 μl. Deionised water with surfactant is used for the reference sample to measure the leakage level of the system which is measured at 99 \pm 8. The dominant contribution to the signal fluctuation comes from electromagnetic noise and the amplifier itself such as thermal and feedback noise. The signal intensity of the 10^4 beads μl^{-1} concentration is measured to be 103 ± 7 , a value that clearly falls within the reference signal fluctuation range. If we define the LOD to lie more than three times the standard deviation (3 σ) above the reference mean then we estimate LOD \approx 124, equivalent to the signal from a 5.6 \times 10⁴ beads μl^{-1} concentration sample. The response curve for the fluorescent beads is quasi-linear up to a concentration of 10^7 beads μl^{-1} (inset of Fig. 8). Our fluorescence detection system at present therefore has a dynamic range spanning some three

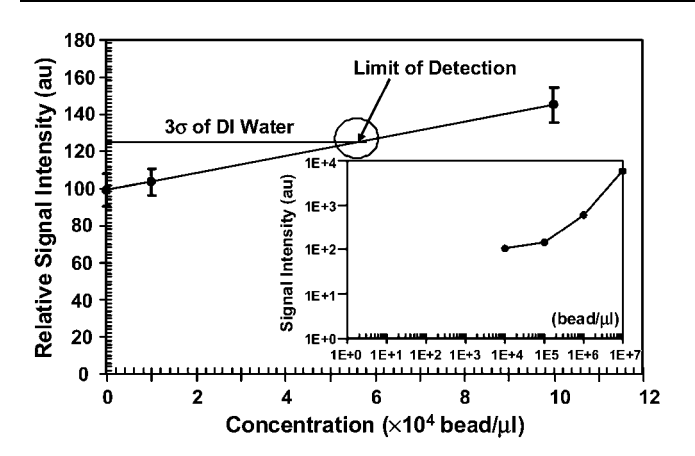


Fig. 8 Spectrally integrated (photodiode detected) fluorescence signal intensity for TransFluoSphere® bead suspensions of increasing concentration measured on-chip using Molecular Vision's fluorescence detection system. The limit of detection at three times the reference (deionised water with surfactant but no beads) signal standard deviation above the reference signal mean is 5.6×10^4 bead μ l⁻¹ (indicated by the horizontal line). The inset graph shows the fluorescence signal intensity over a wider bead concentration range.

orders of magnitude in sample concentration, making it suitable in analytical terms for *in vitro* diagnostic tests where the clinically significant range is generally less than three orders of magnitude.

To compare our LOD result with other reported results, we need some direct/indirect method to quantify the TransFluo-Sphere® bead concentration. To this end, the fluorescence intensity of the beads was compared to the emission of fluorescein, a commonly used fluorophore. A FluoroMax-3 spectrofluorometer was used for the fluorescence measurements with the excitation wavelength for TransFluoSphere® beads set to 500 nm (to mimic the peak emission of the LEDs used in this research). For fluorescein the excitation wavelength was set to the maximum absorption peak wavelength of 490 nm. Integrated fluorescence intensity was then determined by calculating the area of the fluorescence spectrum up to 1/e of the maximum intensity (36.7%).

TransFluoSphere® beads were diluted from the original bead suspension (10^{13} beads ml⁻¹) with DI water while fluorescein (5.52×10^{-22} g per molecules) was diluted with ethanol and the concentration converted to molecules ml⁻¹. Fig. 9 shows the fluorescence spectra for fluorescein and TransFluoSphere® beads with the hatched area representing the integrated fluorescence intensities. By iterative change of the fluorescein concentration it was found that 3.0×10^{14} molecules ml⁻¹ of fluorescein solution and 1.0×10^{10} beads ml⁻¹ of TransFluoSphere® suspension show similar integrated fluorescence intensities. From this result we conclude that a single TransFluoSphere® bead has the equivalent efficiency of $\sim 3 \times 10^4$ fluorescein molecules. In terms of the limit of detection (LOD) of our detection system the previously determined 5.6×10^4 beads μ l⁻¹ thus correspond to a fluorescein concentration of ~ 3 nM.

4.2. Cardiac marker tests

Cardiac marker tests are important to physicians to assess acute coronary syndromes and to identify and manage high-risk patients. There are many markers for assessment of suspected acute myocardial infarction such as CK-MB,

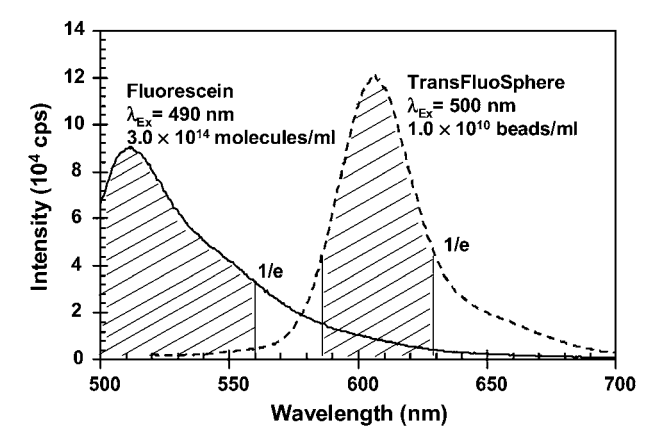


Fig. 9 Fluorescence spectra of 3.0×10^{14} molecules ml $^{-1}$ fluorescein solution (solid line) for an excitation wavelength of 490 nm and 1.0×10^{10} beads ml $^{-1}$ TransFluoSphere® suspension (dashed line) for an excitation wavelength of 500 nm. The hatched area of each spectrum up to 1/e of the maximum intensity represents integrated fluorescence intensities that are similar for the two solutions.

myoglobin, homocysteine, C-reactive protein (CRP), troponin T (cTnT), and troponin I (cTnI). Rapid turnaround of these tests is important and for this reason they would benefit from being performed as point of care tests. In this paper we applied prototype fluorescence immunoassays for two of these, CK-MB and myoglobin, to a microfluidic based system coupled with the optical detection system described above. Depending on the specific antibody reagents applied, the 2-channel microfluidic can be used for two analyses of a single analyte or for the simultaneous measurement of two analytes from a single sample. The latter would be preferable for clinical use but during development the data for each test have been gathered separately to maintain flexibility of experimental design during optimisation of the antibody reagents. Fig. 10 shows typical dose-response curves: the filled circle data and dotted line are for CK-MB and the filled square data and solid line are for myoglobin. Five measurements were made for each concentration and the data points are the means with the error bars representing the standard deviations. The significant signal level at the 0 ng ml⁻¹ concentration for both assays arises from nonspecific binding of the fluorescent beads in the detection chamber (leakage light also contributes to the signal level, see Fig. 8) and would be expected to be reduced with optimisation of the reagent processes. The detection limit for each assay was calculated as the concentration corresponding to the mean plus three standard deviations of the signal for the zero standard. Although more rigorous procedures are applied for tests within a true clinical setting,35 this method is widely used within the diagnostics industry to provide a performance guide during the development of an assay. A figure of 1.5 ng ml⁻¹ was obtained for both myoglobin and CK-MB. Such sensitivity is more than adequate for a myoglobin test where the 95th percentile of a healthy population may extend to 100 ng ml⁻¹ and absolute sensitivity is not critical. For an early stage prototype development, the 1.5 ng ml⁻¹ for CK-MB also compares favourably with a commercial POCT system: Biosite Triage® CK-MB has a detection limit of 1.0 ng ml⁻¹.

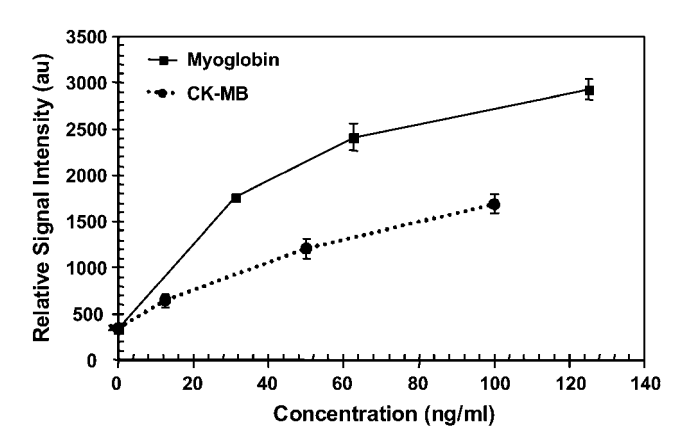


Fig. 10 Fluorescence signal intensity curves measured for increasing concentrations of myoglobin and CK-MB using Molecular Vision's detection system.

Thus despite the significant non-specific binding noted above, the optical detection system is already capable of delivering performance that is close to the requirements of commercial POCT and with improvements in the reagent processes may be expected to achieve these and have capabilities for the measurement of analytes that are present in human plasma at lower concentrations, such as Troponin I.

5. Conclusion

By using low-cost optical components and a microfluidic based system we have demonstrated that it would be practical to achieve the performance required for a POCT system from a design configuration that is simple to use, capable of multiplexed testing to handle a panel of related analytes from a single sample, provides a quantitative output and could be manufactured in volume allowing improved economics.

The work described here was performed using 2-channel single-use disposable microfluidic chips and a fluorescence reader comprising an InGaN based LED (501 nm) light source, an organic or silicon photodiode and a combination of absorptive short and long pass filters and linear and reflective polarisers. Whilst this configuration can potentially be visualised for use in a system such as a hand-held reader plus disposable reagent chips, such is the simplicity of the optical components, particularly as organic LEDs and PDs become more-widely available, that its true benefit would be best realised as a fully integrated disposable, complete with optical components and low-cost electronics mounted on the microfluidic chip. Such a design would avoid some of the disadvantages of POCTs such as the cost of purchasing and maintaining additional equipment, operator training, shelf-space, the proliferation of different readers for different diagnostic panels and the overall dependence on instrumentation and its one-test-at-a-time limitation.

References

- 1 Point of Care Testing, Biophoenix, 2010.
- 2 C. L. Barton, The Future of Cardiovascular Diagnostics: Impact of Technological Advances on Growth Opportunities and Future Market Outlook, 2010.
- 3 Kalorama_In Vitro Diagnostic Tests, 6th edn, 2008.

- 4 Management and Use of IVD Point of Care Test Devices, MHRA Device Bulletin, DB2010(02), February 2010.
- 5 F. Xu, P. Datta, H. Wang, S. Gurung, M. Hashimoto, S. Wei, J. Goettert, R. L. McCarley and S. A. Soper, *Anal. Chem.*, 2007, 79, 9007–9013.
- 6 P. Liu, T. S. Seo, N. Beyor, K. J. Shin, J. R. Scherer and R. A. Mathies, *Anal. Chem.*, 2007, 79, 1881–1889.
- 7 A. Pais, A. Banrjee, D. Klotzkin and I. Papautsky, *Lab Chip*, 2008, 8, 794–800.
- 8 O. Schmidt, M. Bassler, P. Kiesel, C. Knollenberg and N. Johnson, Lab Chip, 2007, 7, 626–629.
- J. A. Chediak, Z. Luo, J. Seo, N. Cheung, L. P. Lee and T. D. Sands, *Sens. Actuators*, A, 2004, 111, 1–7.
- 10 J. B. Edel, N. P. Beard, O. Hofmann, J. C. de Mello, D. D. C. Bradley and A. J. de Mello, *Lab Chip*, 2004, 4, 136–140.
- 11 O. Hofmann, X. Wang, J. C. de Mello, D. D. C. Bradley and A. J. de Mello, *Lab Chip*, 2005, **5**, 863–868.
- 12 A. Llobera, S. Demming, R. Wilke and S. Buttgenbach, *Lab Chip*, 2007, 7, 1560–1566.
- 13 J. Steigert, M. Grumann, T. Brenner, L. Riegger, J. Harter, R. Zengerle and J. Ducree, *Lab Chip*, 2006, 6, 1040–1044.
- 14 O. Hofmann, P. Miller, P. Sullivan, T. S. Jones, J. C. de Mello, D. D. C. Bradley and A. J. de Mello, Sens. Actuators, B, 2005, 106, 878–884.
- 15 X. Wang, O. Hofmann, R. Das, E. M. Barrett, A. J. de Mello, J. C. de Mello and D. D. C. Bradley, *Lab Chip*, 2007, 7, 58–63.
- 16 X. Wang, M. Amatatongchai, D. Nacrapricha, O. Hofmann, J. C. de Mello, D. D. C. Bradley and A. J. de Mello, *Sens. Actuators, B*, 2009, 140, 643–648.
- 17 A. Bhattacharyya and C. M. Klapperich, *Biomed. Microdevices*, 2007, 9 245–251
- 18 G. Marchand, P. Broyer, V. Lanet, C. Delattre, F. Foucault, L. Menou, B. Calvas, D. Roller, F. Ginot, R. Campagnolo and F. Mallard, *Biomed. Microdevices*, 2008, 10, 35–45.
- 19 A. Ymeti, J. Greve, P. V. Lambeck, T. Wink, S. W. F. M. vanHovell, T. A. M. Beumer, R. R. Wijin, R. G. Heideman, V. Subramaniam and J. S. Kanger, *Nano Lett.*, 2007, 7, 394–397.
- 20 J. Xu, D. Suarez and D. S. Gottfried, Anal. Bioanal. Chem., 2007, 389, 1193–1199.
- 21 F. J. Blanco, M. Agirregabiria, J. Berganzo, K. Mayora, J. Elizalde, A. Calle, C. Dominguez and L. M. Lechuga, J. Micromech. Microeng., 2006, 16, 1006–1016.
- 22 C. Albrecht, N. Kaeppel and G. Gauglitz, *Anal. Bioanal. Chem.*, 2008, 391, 1845–1852.
- 23 D. J. Bornhop, J. C. Latham, A. Kussrow, D. A. Markov, R. D. Jones and H. S. Sorensen, *Science*, 2007, 317, 1732–1736.
- 24 T. M. Chinowsky, M. S. Grow, K. S. Johnston, K. Nelson, T. Edwards, E. Fu and P. Yager, *Biosens. Bioelectron.*, 2007, 22, 2208–2215.
- 25 B. N. Feltis, B. A. Sexton, F. L. Glenn, M. J. Best, M. Wilkins and T. J. Davis, *Biosens. Bioelectron.*, 2008, 23, 1131–1136.
- 26 D. Wei, O. A. Oyarzabal, T. S. Huang, S. Balasubramanian, S. Sista and A. L. Simonian, J. Microbiol. Methods, 2007, 69, 78–85.
- 27 G. L. Liu and L. P. Lee, Appl. Phys. Lett., 2005, 87, 074101-074103.
- 28 L. Novak, P. Neuzil, J. Pipper, Y. Zhang and S. Lee, *Lab Chip*, 2007, 7, 27–29.
- 29 O. Hofmann, X. Wang, A. Cornwell, S. Beecher, A. Raja, D. D. C. Bradley, A. J. deMello and J. C. deMello, *Lab Chip*, 2006, 6, 981–987
- 30 A. Mosley, G. Ryu and H. Jiang, 2009, WO 2009/013494 A1.
- 31 K. S. Whitehead, M. Grell, D. D. C. Bradley, M. Jandke and P. Strohriegl, *Appl. Phys. Lett.*, 2000, **76**, 2946–2948.
- 32 M. Grell, M. Redecker, K. Whitehead, D. D. C. Bradley, M. Inbasekaran and E. P. Woo, *Liq. Cryst.*, 1999, **26**, 1403– 1407.
- 33 J. Huang, R. Xia, Y. Kim, J. Dane, O. Hofmann, X. Wang, A. Mosley, A. J. de Mello, J. C. de Mello and D. D. C. Bradley, J. Mater. Chem., 2007, 17, 1043–1049.
- 34 Y. Kim, S. A. Choulis, J. Nelson, D. D. C. Bradley, S. Cook and J. R. Durrant, *J. Mater. Sci.*, 2005, 40, 1371–1376; Y. Kim, S. A. Choulis, J. Nelson, D. D. C. Bradley, S. Cook and J. R. Durrant, *Appl. Phys. Lett.*, 2005, 86, 063502.
- 35 Protocols for Determination of Limit of Detection and Limits of Quantitation, Approved Guideline, EP17-A, Clinical and Laboratory Standards Institute.